Manuscript Details

Abstract

In this work, a comprehensive characterisation and source apportionment of size-segregated aerosol collected using a multistage cascade impactor was performed. The samples were collected during wintertime in Milan (Italy), which is located in the Po Valley, one of the main pollution hot-spot areas in Europe. For every sampling, size-segregated mass concentration, elemental and ionic composition, and levoglucosan concentration were determined. Size-segregated data were inverted using the program MICRON to identify and quantify modal contributions of all the measured components. The detailed chemical characterisation allowed the application of a three-way (3-D) receptor model (implemented using Multilinear Engine) for size-segregated source apportionment and chemical profiles identification. It is noteworthy that - as far as we know - this is the first time that three-way source apportionment is attempted using data of aerosol collected using traditional cascade impactors. Seven factors were identified: wood burning, industry, resuspended dust, regional aerosol, construction works, traffic 1, and traffic 2. Further insights into size-segregated factor profiles suggested that the traffic 1 factor can be associated to diesel vehicles and traffic 2 to gasoline vehicles. The regional aerosol factor resulted to be the main contributor (nearly 50%) to the droplet mode (accumulation sub-mode with modal diameter in the range 0.5-1 µm), whereas the overall contribution from the two factors related to traffic was the most important one in the other size modes (34-41%). The results showed that applying a 3-D receptor model to size-segregated samples allows identifying factors of local and regional origin while receptor modelling on integrated PM fractions usually singles out factors characterised by primary (e.g. industry, traffic, soil dust) and secondary (e.g. ammonium sulphate and nitrate) origin. Furthermore, the results suggested that the information on size-segregated chemical composition in different size classes was exploited by the model to relate primary emissions to rapidly-formed secondary compounds.

Corresponding Author   Roberta Vecchi

Order of Authors   Vera Bernardoni, Miriam Elser, Gianluigi Valli, Sara Valentini, Alessandro Bigi, PAOLA FERMO, Andrea Piazzalunga, Roberta Vecchi

Suggested reviewers   Peter Molnár, Fulvio Amato, claudio Belis, Wioletta Rogula-Kozłowska, Imre SALMA

1   **Size-segregated aerosol in a hot-spot pollution urban area: Chemical composition and three-**

2   **way source apportionment**

3   V. Bernardoni[1], M. Elser[1,#], G. Valli[1], S. Valentini[1], A. Bigi[2], P. Fermo[3], A. Piazzalunga[3,§], R.

4   Vecchi[1,*]

5   [1]Dipartimento di Fisica, Università degli Studi di Milano and INFN-Milan, Milan, Italy

6   [2]Dipartimento di Ingegneria "Enzo Ferrari", Università degli Studi di Modena e Reggio Emilia,

7   Modena, Italy

8   [3]Dipartimento di Chimica, Università degli Studi di Milano, Milan, Italy

9   [#]now at: Swiss Federal Laboratories for Materials Science and Technology, Empa, Dübendorf,

10   Switzerland

11   [§]now at: Water & Life Lab, Entratico (BG), Italy

12

13   *Corresponding Author:

14   Prof. Roberta Vecchi

15   Dipartimento di Fisica

16   Università degli Studi di Milano

17   Via Celoria 16

18   20133 Milan

19   Italy

20   tel: +39 02 50317498

21   email: roberta.vecchi@unimi.it

22

23   **Abstract**

24   In this work, a comprehensive characterisation and source apportionment of size-segregated aerosol

25   collected using a multistage cascade impactor was performed. The samples were collected during

26   wintertime in Milan (Italy), which is located in the Po Valley, one of the main pollution hot-spot

27   areas in Europe.

28   For every sampling, size-segregated mass concentration, elemental and ionic composition, and

29   levoglucosan concentration were determined. Size-segregated data were inverted using the program

30   MICRON to identify and quantify modal contributions of all the measured components.

31   The detailed chemical characterisation allowed the application of a three-way (3-D) receptor model

32   (implemented using Multilinear Engine) for size-segregated source apportionment and chemical

33   profiles identification. It is noteworthy that - as far as we know - this is the first time that three-way

34   source apportionment is attempted using data of aerosol collected using traditional cascade

35   impactors. Seven factors were identified: wood burning, industry, resuspended dust, regional

aerosol, construction works, traffic 1, and traffic 2. Further insights into size-segregated factor profiles suggested that the traffic 1 factor can be associated to diesel vehicles and traffic 2 to gasoline vehicles. The regional aerosol factor resulted to be the main contributor (nearly 50%) to the droplet mode (accumulation sub-mode with modal diameter in the range 0.5-1 μm), whereas the overall contribution from the two factors related to traffic was the most important one in the other size modes (34-41%).

The results showed that applying a 3-D receptor model to size-segregated samples allows identifying factors of local and regional origin while receptor modelling on integrated PM fractions usually singles out factors characterised by primary (e.g. industry, traffic, soil dust) and secondary (e.g. ammonium sulphate and nitrate) origin. Furthermore, the results suggested that the information on size-segregated chemical composition in different size classes was exploited by the model to relate primary emissions to rapidly-formed secondary compounds.

Capsule: detailed chemical characterisation of samples collected by multistage cascade impactor was performed. Application of three-way receptor model allowed obtaining size-segregated source apportionment.

Keywords: Multistage cascade impactor; aerosol size distribution; size-segregated chemical composition; three-way source apportionment; gasoline vehicles; diesel vehicles

1. Introduction

Atmospheric aerosol is a complex mixture of solid and liquid particles suspended in the atmosphere. Atmospheric aerosol has impacts at local scale on health (e.g. Pope and Dockery, 2006), visibility (e.g. Watson, 2002), cultural heritage damage (e.g. Bonazza et al., 2005) and at global scale on the Earth radiation balance (IPCC, 2013). The main parameters determining the aerosol effects are particle sizes and chemical properties, which depend on source emissions and following transformations/reactions in atmosphere (Pöschl, 2005). As examples, size-segregated information can be used to gain further insights into aerosol effects on health (Heal et al., 2012) and can be exploited in perspective to improve Earth radiative transfer models.

Atmospheric aerosol can be separated in several size-ranges and collected for subsequent analysis using multistage cascade impactors. Measurement techniques for the characterisation of different components of size-segregated aerosol have been described in the literature (e.g. Maenhaut et al., 1999 for elemental analysis by Particle-Induced X-ray emission; Viidanoja et al., 2002 for organic and elemental carbon analysis). To provide complete chemical characterisation, sampling on different filter media is mandatory (e.g. Maenhaut et al., 2002; Rogula-Kozłowska, 2016; Salma et

al., 2005). Nevertheless, sampling using cascade impactors is not straightforward, mainly due to the number of samples to deal with. Thus, it can be worthy developing non-destructive, traditional techniques (e.g. ED-XRF) to provide a relatively wide chemical characterisation on the same sample with no need of unconventional laboratory devices (e.g. accelerators).

Information on aerosol sources can be obtained from physical-chemical characterisation of aerosol collected in ambient air e.g. using multivariate receptor models (Hopke, 2016; Viana et al., 2008; and therein cited literature), which allow to retrieve aerosol source contributions, chemical profiles, and temporal trends. Three-way (3-D) source apportionment models (Harshman and Lundy, 1994; Tucker, 1966) can be applied to size- and time-resolved aerosol samples to obtain information on size-segregated source profiles and contributions. Nevertheless, in spite of the importance of exploiting information on size-segregated aerosol composition for source apportionment purposes, studies concerning a comprehensive characterisation of aerosol segregated in more than two size classes coupled to 3-D source apportionment are nearly absent in the literature. Few examples are applications to data collected using a high-resolution time-of-flight mass spectrometer - HR-ToF-MS (Ulbrich et al., 2012) or drum impactors (Li et al., 2013; Peré-Trepat et al., 2007). Nevertheless, the high cost and complex operation of the HR-ToF-AMS and the need of accelerator facilities for the elemental analysis of drum impactor samples (Bukowiecki et al., 2005; Cahill, 1996) strongly limit the spatial and temporal applicability of these techniques.

In this work, a comprehensive characterisation of size-segregated aerosol collected using a multistage cascade impactor was performed quantifying mass by gravimetry, elements by ED-XRF, main inorganic ions and levoglucosan by liquid chromatographic techniques. The detailed size-segregated characterisation allowed the determination of mass and chemical components size distribution at a heavily polluted area (Milan, Italy). Furthermore, a 3-D receptor model (implemented using Multilinear Engine) was applied to obtain size-segregated source profiles and apportionment from samples collected using traditional multistage cascade impactors. As far as we know, this is the first time that 3-D source apportionment is attempted on this kind of data.

2. Materials and Methods

2.1 Sampling

Aerosol was sampled using a multistage cascade impactor collecting particles in 12-stages with nominal cut-off diameter in the range 45 nm - 8.5 μm (SDI, Dekati - more details in Bernardoni et al., 2011a). Samples were collected on coated polycarbonate substrates to avoid particle bouncing among impaction stages. Coating was performed using DS-515 spray by Dekati. Upstream the impactor, a PM10 EPA-equivalent inlet was used. It is noteworthy to recall that EPA inlets are designed to perform a 10 μm cut-off at 16.67 l/min. Considering the SDI flow-rate (11.12 l/min),

106   the expected size-cut of the inlet in this work was calculated to be 12.2 μm.

107   Samplings were performed at an urban background site in the University Campus in the period

108   January-March 2011. Fourteen samplings were performed with a time resolution in the range 24-48

109   h, for a total of 168 polycarbonate foils available for the analysis.

110   During the sampling period, median temperature was 7.4°C (range: -2.7°C to 20.0°C, except for the

111   last three samplings when temperatures up to 24°C were reached). Average wind speed was 0.72

112   m/s. Wind speed higher than 4 m/s were occasionally registered during a Foehn event (15th

113   February). Precipitations occurred during 1 sampling only, with a rate lower than 2 mm/h. The

114   integral precipitation during that sampling was 6.4 mm.

115

116   *2.2 Laboratory analyses*

117   All the substrates were weighed before and after the sampling using an analytical microbalance

118   (precision 1 μg) in an air-conditioned weighing room (T = 20 ± 1°C and R.H. = 50 ± 5%). Before

119   weighing, filters were placed on open but dust-protected sieve-trays for 48 hours in the weighing

120   room for conditioning. The weighing protocol is described in Vecchi et al. (2004). Calibration

121   procedures checked the microbalance performance.

122   Elemental composition (S, Cl, K, Ca, Ti, V, Cr, Mn, Fe, Ni, Cu, Zn, Br, Pb) was determined on all

123   samples using an Energy-Dispersive X-Ray Fluorescence instrument (ED-2000, Oxford) suitably

124   set up for the analysis of samples collected using multistage cascade impactors (details in

125   Bernardoni et al., 2011a). Minimum detection limits were in the range 1-20 ng/sample, depending

126   on the considered element (except for S and Cl: 140 and 89 ng/sample, respectively), corresponding

127   to about 0.1-8.9 ng/m^3 when considering sampling volumes. Uncertainties were estimated in the

128   range 7-15% for most elements and samples.

129   After ED-XRF analysis, which is fully not destructive, all the samples were water extracted for the

130   determination of the main inorganic ions ($SO_4^=$, NO_3^-, NH_4^+, K^+) and levoglucosan. Extraction of

131   each sample was performed using 30 μl methanol and 3 ml MilliQ water, sonicating for 1 h. The

132   main inorganic ions were determined by ion chromatography (details in Piazzalunga et al., 2013).

133   Minimum detection limits were 25 ng/sample for ammonium (0.7-1.6 ng/m^3 depending on sampling

134   volume), 100 ng/sample for sulphate and nitrate (3.2-7.3 ng/m^3), and 170 ng/sample for potassium

135   (5.4-12.3 ng/m^3). Uncertainties were about 10%. Levoglucosan measurements were performed by

136   high-performance liquid chromatography coupled to pulsed-amperometric detection (HPAEC–

137   PAD) (details in Piazzalunga et al., 2010). Minimum detection limit was 11 ng/sample (0.4-0.8

138   ng/m^3) and uncertainties were about 10%.

139

140   *2.3 Modes retrieval by the program MICRON.*

141   For each measured component, size segregated concentration measured by multistage impactors is

142   usually represented as histogram (see Figure 1a). Each bar of the histogram is related to the

143   characteristics of the considered impactor stage and of the collected aerosol as follows: the bar

144   width (represented in log-scale) extends from the cut-off of considered stage and the cut-off of the

145   previous one (i.e. the adjacent stage with higher cut-off); the bar height represents $\Delta m / \Delta \log(d_p)$

146   where Δm is the component mass measured on the considered stage and $\Delta \log(d_p)$ is the difference

147   between the logarithms of the cut-off diameters of the previous and considered stages. When a

148   continuous distribution is of interest, $dm/d(\log(d_p))$ as a function of d_p are represented (note that

149   when $\log(d_p)$ is used, it has to be intended as $\log(d_p/d_{p0})$, where $d_{p0}=1\mu m$, for details see Seinfeld

150   and Pandis, 1998). Nevertheless, a more accurate representation of the original size distribution has

151   to take into account real cut-off curves of the impactor. To this aim, the inversion program

152   MICRON (Wolfenbarger and Seinfeld, 1990) was used to retrieve the original size distribution of

153   the different chemical components for each sampling (see Figure 1b). The inversion is based on a

154   constrained regularisation algorithm. Model inputs are the mass/species concentrations collected on

155   each impaction stage, which are redistributed considering the actual collection efficiency of the SDI

156   impactor (Hillamo, 1994) and the uncertainties on input data. Each inverted $dm/d(\log(d_p))$

157   distribution is then fitted with log-normal functions (see Figure 1c) to retrieve the geometric mean

158   aerodynamic diameter (GMAD), and the different contributions of the modes (Maenhaut et al.,

159   1996).

160

161   ***2.4 Source apportionment***

162   Source apportionment was performed using a vector-matrix decomposition, inspired to the Tucker1

163   model (Tucker, 1966). In this model, each element $x_{i,j,k}$ of the 3-D input matrix representing the M

164   species of the aerosol collected in N stages of a cascade impactor during R samplings is factorised

165   in S (unknown) factors as follows: $x_{i,j,k} = \sum_{p=1}^{S} b_{i,j,p} a_{p,k} + \varepsilon_{i,j,k}$, where $\varepsilon_{i,j,k}$ is the difference between the

166   measured and the modelled concentrations. Different meanings can be attributed to the factorising

167   terms (Ulbrich et al., 2012). In our decomposition, $b_{i,j,p}$ ($1 \leq i \leq N$, $1 \leq j \leq M$, $1 \leq p \leq S$) was an element

168   of an N×M×S array, where each N×M layer represents the size-segregated p-th factor profile and

169   $a_{p,k}$ ($1 \leq k \leq R$) represents the contribution of the p-th factor to the k-th sampling.

170   The model was implemented using Multilinear Engine - ME-2 (Paatero, 1999) and is based on the

171   minimisation of the object function $Q = \sum_i \sum_j \sum_k \frac{\varepsilon_{i,j,k}^2}{\sigma_{i,j,k}^2}$, where $\sigma_{i,j,k}$ is the uncertainty associated to

172   each $x_{i,j,k}$. The function Q previously reported represents the main equation of the model. Further

173   constraints can be applied by adding other terms (auxiliary equations). The conjugate gradient

174 algorithm is used to compute the solution. Non-negativity constraints are implemented by using the

175 well-known technique of pre-conditioning in opposite way for slowing down changes of variables

176 that are about to become negative. Factor scaling indeterminacy can be removed including a priori

177 information on factor matrices. In our case, normalisation was carried out as follows: $\sum_{k} a_{p,k} = 1$ for

178 each factor p.

179 The model was run using strong variables (Paatero 2015). This excluded Cr and Ni. S and $SO_4^=$

180 showed very good correlation and correct stoichiometric ratio. $SO_4^=$ was chosen because of the

181 higher associated explained mass. The choice between K^+ and K was performed considering that

182 they were very well correlated for d≤2.70 μm but K provided significant contribution also in larger

183 size fractions (due to insoluble K related e.g. to potassium oxides in crustal material). Thus, K was

184 chosen as input. Cl resulted with no other tracers in a single factor accounting for few mass thus

185 preventing physical interpretation. Summarising, twelve variables were chosen as input data: K, Ca,

186 Ti, Mn, Fe, Cu, Zn, levoglucosan, $SO_4^=$, NO_3^-, NH_4^+, and mass. It is noteworthy that carbonaceous

187 material was not measured so that unexplained mass (i.e. the difference between the mass and the

188 detected species) ranged from 34% to >95% depending on the sample. Generally, the highest

189 unexplained mass was registered in very small size classes: this was consistent with the small size

190 expected for carbonaceous particles emitted from combustion processes.

191 Data and uncertainties were treated following Polissar et al. (1998). In our case, $\sigma_{i,j,k}$ was the

192 analytical uncertainty associated to the chemical species. Exception was the uncertainty associated

193 to the mass as it was increased to 4-times the mass value. Indeed, mass was considered as "total

194 variable", i.e. it was used to determine factor scaling and for source contribution quantification.

195 Total variable should not have strong influence on the solution, thus it should be always down-

196 weighed (EPA, 2014).

197 Species were measured in 168 samples. Data were arranged into a 3-D matrix representing 12 size

198 classes × 12 species × 14 samplings. Missing data were identified as -999 and were automatically

199 excluded by the program in the computation of the Q function. Due to the unknown number of

200 factors, solutions for different numbers of factors were explored to identify the best solution.

201 Multiple minima are a crucial issue in 3-D models. Thus, the global minimum and a few of the

202 deepest local minima were explored (Paatero, 2000).

203

204 **3. Results and discussion**

205 *3.1 Mass and chemical components size distribution*

206 All the size-segregated data concerning mass and chemical components for all the samplings were

207 inverted using the program MICRON as explained in paragraph 2.3.

For what concerns aerosol mass, two different types of mass size distributions were detected in the measured data (see Figure 2). They mainly differed in the absence (type 1) or presence (type 2) of a detectable Aitken mode at about 100 nm. The presence of the Aitken mode has probably to be ascribed to samples impacted by fresh and local emissions and its absence to a more aged aerosol. Some literature works argued the possibility of vapour condensation during low-pressure impactor sampling due to expansion cooling. Nevertheless, Raabe et al. (1988) did not found it as an issue considering that the lower temperature is reached instantaneously and maintained only for short time (of the order of μs). When present, the Aitken mode accounted on average for 9% of the measured mass.

For $d > 100$ nm, the mass size distribution showed the accumulation mode separated into two sub-modes (condensation mode and droplet mode, e.g. see Seinfeld and Pandis, 1998) and the coarse mode. GMADs for condensation, droplet, and coarse modes were 0.28 μm, 0.72 μm, 4.1 μm, respectively, for mass size distribution type 1; for mass size distribution type 2, GMADs for the three modes were 0.29 μm, 0.71 μm, 3.7 μm. Mode GMADs were very similar to previously literature findings (e.g. Cabada et al., 2004; Salma et al., 2005). Whether no significant differences in mode GMADs were present between the two size distribution types, the relative contribution of condensation and droplet modes was different: indeed, in mass size distribution type 1 the contribution of the droplet mode was significantly higher than in the other case. This observation and the absence of the Aitken mode evidenced the role of aging processes leading to the increase of particle sizes.

Modal distributions for all the measured chemical components were retrieved. Condensation, accumulation, and coarse modes, as well as very large particles were detected for most species, whereas Aitken nuclei mode was detected for levoglucosan, NO_3^-, $SO_4^=$, and K^+. Results concerning these modes GMADs, relative mass concentration (RMC) (when modes were present), and the relative number of cases in which modes occurred were summarised in Table 1. Furthermore, an "intermediate mode" (not shown in Table 1) with 0.9 μm $\leq$ GMAD $\leq$1.2 μm was detected in more than 85% cases for Ca, Ti, Fe, Cu, and in 36% cases for Ni. When present, the intermediate mode accounted for less than 25% of the total mass of the species. An intermediate mode was already found for Ca, Ti, and Fe at urban sites in the literature (Pakkanen et al., 2001; Salma et al., 2005), where coal combustion (not expected to impact the samples presented in this work), regional, and mineral aerosol related to road dust were mentioned as possible origin of the mode.

It is noteworthy that information on the size distribution of chemical components is very important e.g. to provide information useful for the assessment of aerosol health effects and to constrain inputs to Earth radiative transfer models.

242 In Figure 3a, the size distribution for secondary inorganic ions was shown. The droplet mode

243 clearly prevailed on the condensation mode consistently with previous findings in the literature (e.g.

244 Cabada et al., 2004), where gas-phase reactions were identified as responsible for the condensation

245 mode formation. Heterogeneous formation, cloud processing, and growth of the condensation mode

246 were indicated as processes leading to droplet mode increase. In addition, secondary inorganic ions

247 presented the Aitken mode (4% relative contribution $SO_4^=$, 2% for NH_4^+ and NO_3^-). In the literature,

248 direct emission of ultrafine inorganic ions (especially sulphate) were associated to combustion

249 processes, as traffic (e.g. Robert et al., 2007) or wood/pellets burning (Ozgen et al., 2017).

250 In Figure 3b, levoglucosan, K^+, and elemental K concentrations were shown. They are known

251 tracers for wood burning (Kleeman et al., 1999; Simoneit et al., 1999; Viana et al., 2008). As

252 expected, K gave a higher contribution than K^+ because it referred to total (i.e. soluble plus

253 insoluble) potassium concentration in atmospheric aerosol. Focusing on $d_p < 1$ μm, the major

254 contribution for wood burning tracers was found in the accumulation sub-modes (as previously

255 observed for secondary inorganic ions) but here the condensation mode dominated on the droplet

256 mode, indicating different formation processes for particles containing these compounds compared

257 to secondary inorganic ions. Furthermore, the presence of the Aitken mode suggested the likely

258 impact of local (urban) emissions by wood/pellet burning. Indeed, recent literature works reported

259 emissions of ultrafine particles containing levoglucosan by wood stoves and K^+ by wood and pellet

260 stoves (Ozgen et al., 2017). Ultrafine particles containing K and levoglucosan were identified also

261 in ambient aerosol in relationship to residential wood burning (Corsini et al., 2017; Pirjola et al.,

262 2017). For $d_p > 1$ μm, a much higher contribution from K than from K^+ can be noticed indicating the

263 contribution from insoluble potassium to be likely ascribed to crustal elements.

264 Figure 3b and Figure 3c represented markers wood burning and traffic sources (among the main

265 sources identified in the Milan urban area in previous works – e.g. Bernardoni et al., 2011b). It is

266 noteworthy that the size distributions for tracers of the two sources are completely different.

267 Opposite, smaller differences are registered among species considered as tracers for the same

268 source. Thus, 3-D receptor modelling was applied trying to exploit these differences to gain further

269 details on emission sources.

270

3.2 Receptor model results

272 The Tucker 1 model was implemented in ME-2 as explained in paragraph 2.4. Receptor models are

273 always affected by multiple solutions for what concerns the possible number of factors, scaling

274 indeterminacy, local minima, and possibly rotations (not an issue in 3-D models). Some

275 mathematical parameters were checked to identify a range of possible solution (expected vs.

276 computed Q value, residuals distribution, and input values reconstruction) (e.g. Belis et al., 2014,

277 Paatero, 2000). All these parameters were evaluated and 5-8 factors were identified as best choices.

278 Nevertheless, mathematics is not enough to determine the right number of factors and the

279 possibility of data interpretation guides the definitive choice (Hopke, 2016; Paatero, 2000). Finally,

280 the 7-factor solution was identified as the best one. The effects of different choices for factor

281 number will be discussed at the end of the paragraph.

282 Factor profiles (total mass of each species normalised to the mass in the factor) and the percent of

283 the species associated to each factor, as well as the mass size distribution of the factors were

284 represented in Figure 4. The mass size distribution was represented both using histogram

285 representation of the ME-2 output and mode representation obtained from data inversion and modes

286 retrieval. In this way, it was possible gaining information on the mass modes GMADs and modes

287 relative contribution to each factor (Table 2). Detailed size-segregated profiles were reported in

288 Figure 5 with histogram representation of the size-segregated relative contribution of the species to

289 the identified factors. In Figure 5, normalisation was carried out to the total average concentration

290 of each species (analogous to percent species for size-segregated representation). Results given in

291 Figure 4, Figure 5, and Table 2 were the bases for factor identification, as explained in the

292 following. Mode-segregated source apportionment for the whole campaign was summarised in

293 Figure 6.

294 The factor identified as "wood burning" was an important contributor to levoglucosan (37%) and at

295 a lesser extent K, well-known tracers for this source, as well as for $SO_4^=$ which was identified as

296 directly emitted by both wood and pellets burning in the literature (e.g. Chandrasekaran et al., 2011;

297 Iinuma et al., 2007). In Figure 5, the contribution of these species was detected also in the ultrafine

298 range and their presence related to residential wood burning as mentioned before. Wood burning

299 factor accounted for 13% of the measured mass. The mass was mainly concentrated in the

300 condensation and droplet modes (96% in total), whereas the remaining 4% was in the Aitken mode.

301 It should be noticed that the mass associated to this source has to be considered as accounting only

302 for local (urban) wood burning contribution. Indeed, a regional contribution from wood burning

303 should be also expected, as 36% of levoglucosan was associated to the regional aerosol factor (see

304 later).

305 The factor identified as "industry" was the main contributor to Zn (35%), which has been identified

306 as a marker for industrial emissions in previous works in the area (e.g. Bernardoni et al., 2011b;

307 Marcazzan et al., 2003). The industry factor accounted on average for 8% of the measured mass.

308 Most of the mass (58%) was contained in the condensation mode, this being among the main

309 contributors to the mass measured in this mode (18%).

310 The factor identified as "resuspended dust" was an important contributor to Ti (27%) and Ca (21%)

311 concentrations. Nevertheless, also components of anthropogenic origin were present and the factor

312   size distribution was characterised in nearly equal parts by fine (<1μm) and coarse particles (54%

313   and 46%, respectively), thus suggesting that anthropogenic particles previously deposited in the

314   ground are resuspended (e.g. by atmospheric agents) together with soil particles. This factor

315   accounted on average for 13% of the measured mass, and it was one of the two main contributors to

316   the coarse mode and very large particles (22%).

317   The factor identified as "regional aerosol" was the main single contributor to the measured

318   concentration of nitrate (52%), sulphate (35%), and ammonium (49%). It can be assumed that these

319   ions were entirely in the form of ammonium sulphate and ammonium nitrate as they were

320   chemically balanced in the profile within 5%. As previously mentioned, this factor was responsible

321   for high contributions to levoglucosan (36%) and K (24%) (tracers for wood burning), and to Fe

322   (22%) and Cu (22%) (tracers for traffic) indicating that this factor was not only associated to

323   secondary aerosol, but also to non-local (aged) contributions from primary sources. The regional

324   aerosol factor was the main contributor to the total measured mass (31%) and to the droplet mode

325   (50%), where 81% of the mass of the factor was found. No contribution from the regional aerosol

326   factor was registered in the Aitken mode, mainly because particles in such mode are typically

327   associated to fresh emissions and tend to coagulate towards the accumulation mode in short times.

328   Particle aging further increases particle size, thus justifying the predominance of the droplet mode.

329   Therefore, the absence of a contribution in the Aitken mode and the small contribution to the

330   condensation mode (9%) were further confirmations of the regional origin of this factor.

331   The factor identified as "construction works" was the main single contributor to the Ca measured

332   concentrations (31%). An association between Ca and construction works at the sampling site was

333   already identified in previous works (Bernardoni et al., 2011b; Vecchi et al., 2009). Its average

334   contribution to the measured mass was 7%. This factor contributed to 22% of the mass measured in

335   the coarse and very large particle modes, where 49% of the mass associated to this factor was

336   found. The coarse/very large particles contribution was ascribed to soil/construction material

337   movement, whereas the contribution to the other modes was related mainly to construction

338   machinery exhaust. It is noteworthy that construction works were locally carried out at the

339   Department of Physics during the measurements period, thus justifying the high (32%) - and quite

340   unexpected - contribution of construction works to the Aitken mode.

341   Two factors were associated to traffic sources and named "traffic 1" and "traffic 2". They showed

342   very similar profiles, and they were both important contributors to Fe and Cu (overall 44%), Mn

343   (overall 52%), and Ca (overall 32%). Fe and Cu are widely used as markers for traffic sources in

344   source apportionment studies (Pant and Harrison, 2013; Viana et al., 2008). Mn and Ca are reported

345   to have multiple sources, including traffic. As examples, Crilley et al. (2017) found important

346   contribution of Mn from traffic in PM10, Amato et al. (2011) identified traffic as a major

347 responsible of Mn concentration in the coarse fraction; Ca is often found in traffic source profiles

348 due to traffic-related resuspension or to the contribution of lubricating oils (Viana et al., 2008). It is

349 noteworthy that the two factors did not represent "traffic exhaust" and "traffic non-exhaust"

350 contributions, as the markers for non-exhaust emissions were present in both factors. As for size

351 distributions, the mass of both factors was mainly concentrated in the two accumulation sub-modes

352 (61% for traffic 1 and 69% for traffic 2). In both factors, 23-24% of the mass of the factor was

353 concentrated in the coarse mode, but traffic 2 showed a further 12% mass contribution to very large

354 particles.

355 The main differences between the two factor profiles were higher contributions from nitrate,

356 ammonium, Mn, and Ti in traffic 2 and from Zn in traffic 1. Little information is present in the

357 literature for what concerns elemental tracers for gasoline and diesel vehicles separately. Lin et al.

358 (2005) evidenced that diesel emissions contributed more than gasoline to the Zn concentrations in

359 ultrafine particles, whereas gasoline was a stronger emitter of ultrafine Mn and Cu. Wang and

360 Hopke (2013) identified that a "Gasoline vehicle" factor by PMF by analysis on PM2.5 samples

361 collected in California was the main responsible of Mn concentration. Link et al. (2017) reported

362 that vehicles equipped with three-way catalyst system (gasoline and liquid petroleum gasoline) have

363 the potential for forming NH_4NO_3 aerosol rapidly and in high yields in presence of OH radicals. In

364 Figure 7, size-segregated distribution of Cu, Mn, and Zn in traffic 1 and traffic 2 factor profiles are

365 shown in histogram representation. Normalisation was carried out setting to 1 the total mass of the

366 single species in each profile. Log-scale was used also for the y-axis to allow better identification of

367 the species contributions to the small-diameter (d ≤ 155 nm) cut-off stages (which were in any case

368 a low fraction of the total mass of the species). It is noteworthy that Zn relative contribution in these

369 stages was higher for traffic 1 (7.3% vs. 3.1% in traffic 2), whereas Cu (6.9%) and Mn (3.9%) were

370 higher for the traffic 2 factor (1.0% Cu and 1.3% Mn in traffic1 factor profile). Furthermore, traffic

371 2 showed 29% contribution from nitrate in the factor profiles (Figure 4).

372 All these pieces of information gave indication of a tentative assignment of traffic 1 to diesel

373 vehicles and traffic 2 to gasoline vehicles contributions. A more detailed insight into these factors

374 showed that traffic 1 factor accounted for 18% of the total measured mass and it was characterised

375 by 83% relative unexplained mass (i.e. the difference between the mass and the sum of the species

376 in the profile), whereas traffic 2 factor accounted for 10% of the total measured mass but the

377 relative unexplained mass was only 51%. For diesel vehicles not equipped with anti-particulate

378 filter, exhaust emissions are known to be at least one order of magnitude higher than gasoline

379 exhaust emissions (e.g. May et al., 2014). It is noteworthy (e.g. Schauer et al., 2006) that the

380 dominant component in exhaust emissions is carbonaceous material which was not detected in this

381 work. Thus, the stronger exhaust contribution expected for diesel vehicles can justify the higher

unexplained mass detected in the traffic 1 factor. Considering that diesel vehicles include also heavy duty vehicles and that such vehicles have a higher potential of dust resuspension, assigning traffic 1 factor to diesel vehicles could justify also the presence of the very large particles in this factor and not in traffic 2.

Traffic 1 and traffic 2 overall contributions made traffic the most important source of particle mass in all modes but the droplet one, where the contribution from the regional aerosol factor was dominant. The overall contribution of the two traffic factors (28%) might appear higher than in past studies in the area (e.g. Bernardoni et al., 2011b where a contribution of 16% was reported during wintertime for PM_{10} samples). Nevertheless, in Bernardoni et al. (2011b) most of secondary ions were accounted for in "secondary sulphate" and "secondary nitrates" factors: thus, the other factors (including traffic) included mainly primary contributions. Opposite, in this work the analysis on size-segregated samples showed secondary aerosol to be partially explained by specific urban sources. Amato et al. (2016) presented a source apportionment study on PM_{10} data collected in Milan and found an overall 16% contribution for vehicle exhaust and non-exhaust and further 14% vehicle nitrate contribution from NO_x emission inventory. Thus, the overall traffic contribution resulted very similar to the value obtained in the current work. All these results evidenced the ability of source apportionment applied to size-segregated samples to relate at least part of the secondary aerosol to specific sources.

Likely the information on chemical composition in different size classes was exploited by the model to relate primary emissions to rapidly-formed secondary compounds. In the regional aerosol factor only 7% of the total nitrate, 13% of sulphate, and 8% of ammonium were found in the four lowest size-classes. In most of other factors, different size distributions were found for secondary compounds. As examples, focusing on the four lowest size classes in the histograms in figure 5, 42% and 41% of the total nitrate in each factor was found in this size range for industry and resuspended dust, respectively, whereas 19% and 17% was found for traffic 1 and wood burning, respectively.

For what concerns other possible solutions obtained running the ME-2 model, 6-factor solution was excluded because the contributions from "industry" and "construction works" factors mixed in a unique ("other anthropogenic") factor. Increasing to 8 factors, the additional factor could not be identified, as no chemical species tracer for known sources could be detected.

Finally, it should be noticed that the main features of the model output (i.e. separation of local vs. regional contributions; ability to identify separate factors associated to gasoline and diesel vehicles) are related to sample features (i.e. size-segregation and detailed chemical characterisation), thus they are not impacted by meteorological conditions. Nevertheless, the latter can affect the relative

416 contribution of the different sources and must be considered when sampling for monitoring

417 purposes – out of the scope of this manuscript – is carried out.

418

419 **4. Conclusions**

420 A study of size-segregated aerosol sampled by SDI multistage impactor was carried out during

421 wintertime in the Milan urban area, which is located in the Po Valley, one of the major pollution

422 hot-spots in Europe.

423 The samples were characterised for mass concentration, and elemental and inorganic ionic

424 composition. Data inversion by the program MICRON and interpolation by log-normal functions

425 allowed detecting and quantifying aerosol modes. Three or four modal mass size distributions were

426 identified in the samples. In all cases, the highest fraction of the mass was found in the

427 accumulation mode.

428 Similarities in size distributions of source tracers suggested the possibility to perform source

429 apportionment. Three-way source apportionment was performed by implementing the Tucker 1

430 model in ME-2. Seven factors were identified, namely wood burning, industry, resuspended dust,

431 construction works, regional aerosol, traffic 1 and traffic 2. It is interesting to note that in previous

432 studies performed in the area on PM_{10} samples, factors related to primary emissions or secondary

433 formation were identified. Opposite, performing the analysis on size-segregated samples led to the

434 identification of local and regional factors. Indeed, running the model on size-segregated samples

435 allowed ascribing part of the secondary compounds to local factors (e.g. traffic 1 and 2, wood

436 burning) probably due to rapid formation of secondary particles in smaller size classes than

437 secondary particles in regional (aged) aerosol. The regional aerosol factor was characterised by a

438 high presence of secondary compounds, but not-negligible contributions primary source tracers (e.g.

439 Cu, Fe, levoglucosan) were also present. The regional aerosol factor prevailed in the droplet mode,

440 whereas the overall contribution from the two traffic sources dominated in the other size fractions.

441 Further insights into the size-segregated profile suggested that the traffic 1 factor could be likely

442 associated to diesel vehicles and the traffic 2 to gasoline vehicles.

443 It is noteworthy that 3-D source apportionment studies on aerosol separated in a number of size

444 classes are nearly absent in the literature. The study presented here showed the possibility to apply

445 3-D source apportionment studies to samples collected with multistage cascade impactors. Such

446 samples can be analysed with traditional techniques (opposite to high-time resolved samples, which

447 usually require to be analysed at accelerator facilities) and do not need dedicated instrumentation

448 other than the sampler. In perspective, these features open the way to more frequent space-

449 distributed size-segregated source apportionment studies, which are of primary importance to

450 optimise the effectiveness of future abatement strategies and to improve Earth radiation balance

451 models.

452

453 **Acknowledgements**

References

461 **References**

462 Amato, F., Viana, M., Richard, A., Furger, M., Prévôt, A. S. H., Nava, S., Lucarelli, F.,

463 Bukowiecki, N., Alastuey, A., Reche, C., Moreno, T., Pandolfi, M., Pey, J., and Querol, X. (2011).

464 Size and time-resolved roadside enrichment of atmospheric particulate pollutants. Atmospheric

465 Chemistry and Physics, 11, 2917-2931

466

467 Amato, F., Alastuey, A., Karanasiou, A., Lucarelli, F., Nava, S., Calzolai, Escrig A., Monfort E.,

468 Sanfelix V., Gianelle V.L., Colombi C., Alves, C., Custódio, D., Nunes, T., Cerqueira, M., Pio, C.,

469 Eleftheriadis, K., Diapouli, E., Reche, C., Minguillón, M. C., Manousakas, M.-I., Maggos, T.,

470 Vratolis, S., Harrison, R. M., and Querol, X. (2016). Non-exhaust contributions to PM levels in 5

471 EU cities. 10th International Conference on Air Quality - Science and Application, Milan, Italy, 14-

472 18 March 2016. https://drive.google.com/drive/folders/0B2iFZ3L-H5pRbGN4Q2NaeGNmQU0

473

474 Belis, C.A., Larsen, B.R., Amato, F., El Haddad, I., Favez, O., Harrison, R.M., Hopke, P.K., Nava,

475 S., Paatero, P., Prévôt, A., Quass, U., Vecchi, R., and Viana, M. (2014). European Guide on Air

476 Pollution Source Identification with Receptor Models. EUR 26080 – Joint Research Centre –

477 Institute for Environment and Sustainability. Luxembourg: Publications Office of the European

478 Union.

479

480 Bernardoni, V., Cuccia, E., Calzolai, G., Chiari, M., Lucarelli, F., Massabò, D., Nava, S., Prati, P.,

481 Valli, G., and Vecchi, R. (2011a). ED-XRF set-up for size-segregated aerosol samples analysis. X-

482 Ray Spectrometry, 40, 79-87

483

484 Bernardoni, V., Vecchi, R., Valli, G. Piazzalunga, A., and Fermo, P. (2011b). PM10 source

485 apportionment in Milan (Italy) using time-resolved data. The Science of the Total Environment,

486 409, 4788-4795

487

488 Bonazza, A., Sabbioni, C., and Ghedini, N. (2005). Quantitative data on carbon fractions in

489 interpretation of black crusts and soiling on European built heritage. Atmospheric Environment, 39,

490 2607-2618

491

492 Bukowiecki, N., Hill, M., Gehrig, R., Lienemann, P., Zwicky, C. N., Hegedüs, F., Falkenberg, G.,

493 Weingartner, E., and Baltensperger, U. (2005). Trace metals in ambient air: hourly size segregated

494 mass concentrations determined by synchrotron-XRF. Environmental Science and Technology, 39,

495 5754–5762

15

496

497   Cabada, J.C., Rees, S., Takahama, S., Khlystov, A., Pandis, S.N., Davidson, C.I., and Robinson,

498   A.L. (2004). Mass size distributions and size resolved chemical composition of fine particulate

499   matter at the Pittsburgh supersite. Atmospheric Environment, 38, 3127-3141

500

501   Cahill, T.A. (1996). Climate Forcing by Anthropogenic Aerosols: The Role for PIXE. Nuclear

502   Instruments and Methods in Physics Research B: Beam Interactions with Materials and Atoms,

503   109/110, 402-406

504

505   Chandrasekaran, S.R., Laing, J.R., Holsen, T.M., Raja, S., and Hopke, P.K. (2011). Emission

506   Characterization and Efficiency Measurements of High-Efficiency Wood Boilers. Energy Fuels, 25,

507   5015–5021

508

509   Corsini, E., Vecchi, R., Marabini, L., Fermo, P., Becagli, S., Bernardoni, V., Caruso, D., Corbella,

510   L., Dell'Acqua, M., Galli, C.L., Lonati, G., Ozgen, S., Papale, A., Signorini, S., Tardivo, R., Valli,

511   G., and Marinovich, M. (2017). The chemical composition of ultrafine particles and associated

512   biological effects at an alpine town impacted by wood burning. Science of the Total Environment,

513   587-588, 223-231

514

515   Crilley, L.R., Lucarelli, F., Bloss, W.J., Harrison, R.M., Beddows, D.C., Calzolai, G., Nava, S.,

516   Valli, G., Bernardoni, V., and Vecchi, R. (2017). Source apportionment of fine and coarse particles

517   at a roadside and urban background site in London during the 2012 summer ClearfLo campaign.

518   Environmental Pollution, 220, 766-778

519

520   EPA (2014). EPA Positive Matrix Factorization (PMF) 5.0 Fundamentals and User Guide.

521   EPA/600/R-14/108, April 2014. https://www.epa.gov/sites/production/files/2015-

522   02/documents/pmf_5.0_user_guide.pdf

523

524   Harshman, R. A. and Lundy, M. E. (1994). PARAFAC – Parallel Factor-Analysis. Computational

525   Statistics & Data Analysis, 18, 39–72

526

527   Heal, M.R., Kumar, P., and Harrison, R.M. (2012). Particles, air quality, policy and health.

528   Chemical Society Reviews, 41, 6606-6630

529

530 Hillamo, R. E. (1994) Development of inertial impactor size spectroscopy for atmospheric aerosols.

531 Ph.D. thesis

532

533 Hopke, P.K. (2016). Review of receptor modeling methods for source apportionment. Journal of the

534 Air & Waste Management Association, 66, 237-259

535

536 Iinuma, Y., Brüggemann E., Gnauk T., Müller K., Andreae M. O., Helas G., Parmar R., and

537 Herrmann H. (2007). Source characterization of biomass burning particles: The combustion of

538 selected European conifers, African hardwood, savanna grass, and German and Indonesian peat.

539 Journal of Geophysical Research, 112, D08209

540

541 IPCC (2013). Climate Change 2013: The Physical Science Basis. Contribution of Working Group I

542 to the Fifth Assessment Report of the Intergovernmental Panel on Climate Change [Stocker, T.F.,

543 D. Qin, G.-K. Plattner, M. Tignor, S.K. Allen, J. Boschung, A. Nauels, Y. Xia, V. Bex and P.M.

544 Midgley(eds.)]. Cambridge University Press, Cambridge, United Kingdom and New York, NY,

545 USA, 1535 pp

546

547 Kleeman, M.J., Schauer, J. J., and Cass, G. R. (1999). Size and Composition Distribution of Fine

548 Particulate Matter Emitted from Wood Burning, Meat Charbroiling, and cigarettes. Environmental

549 Science and Technology, 33, 3516-3523

550

551 Li, N., Hopke, P.K., Kumar, P., Cliff, S.S., Zhao, Y., and Navasca, C. (2013). Source

552 apportionment of time- and size-resolved ambient particulate matter. Chemometrics and Intelligent

553 Laboratory Systems, 129, 15–20

554

555 Lin, C.-C., Chen, S.-J., Huang, K.-L., Hwang, W.-I., Chang-Chien, G.-P., and Lin, W.-Y. (2005).

556 Characteristics of metals in nano/ultrafine/fine/coarse particles collected beside a heavily Trafficked

557 road. Environmental Science and Technology, 39, 8113–8122

558

559 Link, M.F., Kim, J., Park, G., Lee, T., Park, T., Bin Babar, Z., Sung, K., Kim, P., Kang, S., Soo

560 Kim, J., Choi, Y., Son, J., Lim, H.-J., and Farmer, D.K. (2017). Elevated production of NH4NO3

561 from the photochemical processing of vehicle exhaust: Implications for air quality in the Seoul

562 Metropolitan Region. Atmospheric Environment, 156, 95-101

563

564 Maenhaut, W., Hillamo, R., Mäkelä, T., Jaffrezo, J.-L., Bergin, M.H., and Davidson, C.I. (1996). A

565 new cascade impactor for aerosol sampling with subsequent PIXE analysis. Nuclear Instruments
566 and Methods in Physics Research Section B: Beam Interactions with Materials and Atoms, 109-
567 110, 482-487
568
569 Maenhaut, W., Jaffrezo, J.-L, Hillamo, R.E, Mäkelä, T, and Kerminen, V.-M. (1999). Size-
570 fractionated aerosol composition during an intensive 1997 summer field campaign in northern
571 Finland. Nuclear Instruments and Methods in Physics Research Section B: Beam Interactions with
572 Materials and Atoms, 150, 345-349
573
574 Maenhaut, W., Cafmeyer, J., Dubtsov, S., and Chi, X. (2002). Detailed mass size distributions of
575 elements and species, and aerosol chemical mass closure during fall 1999 at Gent, Belgium.
576 Nuclear Instruments and Methods in Physics Research Section B: Beam Interactions with Materials
577 and Atoms, 189, 238-242
578
579 Marcazzan, G.M., Ceriani M., Valli G., and Vecchi R. (2003). Source apportionment of PM10 and
580 PM2.5 in Milan (Italy) using receptor modelling. Science of the Total Environment, 317, 137-147
581
582 May, A., Nguyen, N., Presto, A., Gordon, T., Lipsky, E., Karve, M., Gutierrez, A., Robertson, W.,
583 Zhang, M., Brandow, C., Chang, O., Chen, S., Cicero-Fernandez, P., Dinkins, L., Fuentes, M.,
584 Huang, S., Ling, R., Long, J., Maddox, C., Massetti, J., McCauley, E., Miguel, A., Na, K., Ong, R.,
585 Pang, Y., Rieger, P., Sax, T., Truong, T., Vo, T., Chattopadhyay, S., Maldonado, H., Maricq, M.,
586 and Robinson, A. (2014). Gas- and particle-phase primary emissions from in-use, on-road gasoline
587 and diesel vehicles. Atmospheric Environment, 88, 247-260
588
589 Ozgen, S., Becagli, S., Bernardoni, V., Caserini, S., Caruso, D., Corbella, L., Dell'Acqua, M.,
590 Fermo, P., Gonzalez, R., Lonati, G., Signorini, S., Tardivo, R., Tosi, E., Valli, G., Vecchi, R., and
591 Marinovich, R. (2017). Analysis of the chemical composition of ultrafine particles from two
592 domestic solid biomass fired room heaters under simulated real-world use. Atmospheric
593 Environment 150, 87-97
594
595 Paatero, P. (1999). The multilinear engine — a table-driven least squares program for solving
596 multilinear problems, including the n-way parallel factor analysis model. Journal of Computational
597 and Graphical Statistics, 8:4, 854-888
598
599 Paatero, P. (2000). User's Guide for the Multilinear Engine Program "ME-2" for Fitting Multilinear

600   and Quasi-Multilinear Models. University of Helsinki: Helsinki, Finland

601

602   Paatero, P. (2015). User's Guide for Positive Matrix Factorization Programs PMF2 and PMF3, Part

603   1–2: Tutorial. University of Helsinki: Helsinki, Finland (update 31 March 2015)

604

605   Pakkanen, T.A., Kerminen, V.-M. K., Korhonen, C.H., Hillamo, R.H., Aarnio, P., Koskentalo, T.,

606   and Maenhaut, W. (2001). Use of atmospheric elemental size distributions in estimating aerosol

607   sources in the Helsinki area. Atmospheric Environment, 39, 5363-5374

608

609   Pant, P., and Harrison, R.M. (2013). Estimation of the contribution of road traffic emissions to

610   particulate matter concentrations from field measurements: A review. Atmospheric Environment,

611   77, 78-97

612

613   Peré-Trepat, E., Kim, E., Paatero, P., and Hopke, P.K. (2007). Source apportionment of time and

614   size resolved ambient particulate matter measured with a rotating DRUM impactor. Atmospheric

615   Environment, 41, 5921–5933

616

617   Piazzalunga, A., Fermo, P., Bernardoni, V., Vecchi, R., Valli, G., and De Gregorio, M.A. (2010). A

618   simplified method for levoglucosan quantification in wintertime atmospheric particulate matter by

619   high performance anion-exchange chromatography coupled with pulsed amperometric detection.

620   International Journal of Environmental Analytical Chemistry, 90, 934–947.

621

622   Piazzalunga, A., Bernardoni, V., Fermo, P., and Vecchi, R. (2013). Optimisation of analytical

623   procedures for the quantification of ionic and carbonaceous fractions in the atmospheric aerosol and

624   applications to ambient samples. Analytical and Bioanalytical Chemistry, 405, 1123- 1132

625

626   Pirjola, L., Niemi, J.V., Saarikoski, S., Aurela, M., Enroth, J., Carbone, S., Saarnio, K.,

627   Kuuluvainen, H., Kousa, A., Rönkkö, T., and Hillamo, R. (2017). Physical and chemical

628   characterization of urban winter-time aerosols by mobile measurements in Helsinki, Finland.

629   Atmospheric Environment, 158, 60-75

630

631   Polissar, A.V., Hopke, P.K., Paatero, P., Malm, W.C., and Sisler, J.F. (1998). Atmospheric aerosol

632   over Alaska: 2. Elemental composition and sources. Journal of Geophysical Research, 103, 19045-

633   19057

634

635   Pope, C.A. III, and Dockery, D.W. (2006). Health Effects of Fine Particulate Air Pollution: Lines

636   that Connect. Journal of Air & Waste Management Association, 56, 709-742

637

638   Pöschl, U. (2005). Atmospheric Aerosols: Composition, Transformation, Climate and Health

639   Effects. Angewandte Chemie International Edition, 44, 7520-7540

640

641   Raabe, O.G., Braaten, D.A., Axelbaum, R.L., Teague, S., and Cahill, T. (1988). Calibration studies

642   of the DRUM impactor. Journal of Aerosol Science, 19, 183-195

643

644   Robert, M. A., Kleeman, M.J., and Jakober, C.A. (2007). Size and Composition Distributions of

645   Particulate Matter Emissions: Part 2—Heavy-Duty Diesel Vehicles. Journal of the Air & Waste

646   Management Association, 57, 1429-1438

647

648   Rogula-Kozłowska, W. (2016). Size-segregated urban particulate matter: mass closure, chemical

649   composition, and primary and secondary matter content. Air Quality, Atmosphere and Health, 9,

650   533-550

651

652   Salma, I., Ocskay, R., Raes, N., and Maenhaut, W. (2005). Fine structure of mass size distributions

653   in an urban environment. Atmospheric Environment, 39, 5363-5374

654

655   Schauer, J.J., Lough G.C., Shafer M.M., Christensen W.F., Arndt M.F., DeMinter J.T., and Park, J.-

656   S. (2006). Characterization of Metals Emitted from Motor Vehicles. Research Report 133. Health

657   Effects Institute, Boston MA

658

659   Seinfeld, J.H., and Pandis, S.N. (1998). Atmospheric Chemistry and Physics from air pollution to

660   climate change. New York. John Wiley and Sons, Incorporated

661

662   Simoneit, B.R.T., Schauer, J.J., Nolte, C.G., Oros, D.R., Elias, V.O., Fraser, M.P., Rogge, W.F.,

663   and Cass, G.R. (1999). Levoglucosan, a tracer for cellulose in biomass burning and atmospheric

664   particles. Atmospheric Environment, 33, 173-182.

665

666   Tucker, L. R. (1966). Some Mathematical Notes on 3-Mode Factor Analysis. Psychometrika, 31,

667   279–311

668

669   Ulbrich, I. M., Canagaratna, M. R., Cubison, M. J., Zhang, Q., Ng, N. L., Aiken, A. C., and

670 Jimenez, J. L. (2012). Three-dimensional factorization of size-resolved organic aerosol mass spectra

671 from Mexico City. Atmospheric Measurement Techniques, 5, 195-224.

672

673 Vecchi R., Marcazzan G., Valli G., Ceriani M., and Antoniazzi C. (2004). The role of atmospheric

674 dispersion in the seasonal variation of PM1 and PM2.5 concentration and composition in the urban

675 area of Milan (Italy). Atmospheric Environment, 38, 4437-4446

676

677 Vecchi R., Bernardoni V., Fermo P., Lucarelli F., Mazzei F., Nava S., Prati P., Piazzalunga A., and

678 Valli G. (2009). 4-hours resolution data to study PM10 in a "hot spot" area in Europe.

679 Environmental Monitoring and Assessment, 154, 283-300.

680

681 Viana, M., Kuhlbusch, T.A.J., Querol, X., Alastuey, A., Harrison, R.M., Hopke, P.K., Winiwarter,

682 W., Vallius, M., Szidat, S., Prévôt, A.S.H., Hueglin, C., Bloemen, H., Wåhlin, P., Vecchi, R.,

683 Miranda, A.I., Kasper-Giebl, A., Maenhaut W., and Hitzenberger R. (2008). Source apportionment

684 of particulate matter in Europe: A review of methods and results. Journal of Aerosol Science 39,

685 827-849

686

687 Viidanoja, J., Kerminen, V.-M., and Hillamo, R. (2002). Measuring the size distribution of

688 atmospheric organic and black carbon using impactor sampling coupled with thermal carbon

689 analysis: Method development and uncertainties. Aerosol Science and Technology, 36, 607-616.

690

691 Wang Y., and Hopke P.K. (2013). A ten–year source apportionment study of ambient fine

692 particulate matter in San Jose, California. Atmospheric Pollution Research, 4, 398-404

693

694 Watson J.G. (2002). Visibility: Science and Regulation. Journal of Air & Waste Management

695 Association 52, 628–713

696

697 Wolfenbarger, J.K., and Seinfeld, J.H. (1990). Inversion of size distribution data. Journal of Aerosol

698 Science, 21, 227-247

Figure captions

Figure 1: example of modes reconstruction: a) histogram representation obtained from data measured on each impaction stage; b) data inversion by the program MICRON; c) modes interpolation. The example is referred to the mass size distribution of one of the collected samples.

Figure 2: average type 1 and type 2 mass size distributions

Figure 3: average size distribution for secondary ions (a), wood burning markers (b), traffic markers (c)

Figure 4: left panel: factor profiles (black bars) and percent species (grey dots); right panel: factor mass size distributions

Figure 5: histogram representation of the size-segregated relative contribution of the species to the identified factors. Normalisation was carried out to the total average concentration of each species. For each species, x-axis represents $log(d_p)$ and the x-axis scale is the same as histograms in figure 1 and figure 4. Cut-off size for each represented stage (i.e. left-end of coloured bars) are reported in the legend.

Figure 6: mode-segregated source apportionment. Sum of percentages is 100%±1% due to number rounding.

Figure 7: histogram representation of size-segregated distribution of (a) Cu, (b) Mn, and (c) Zn in the traffic 1 and traffic 2 factors profile. Normalisation to the total concentration of the species to each factor profile was carried out. For each component, x-axis represents $log(d_p)$ and the x-axis scale is the same as histograms in figure 1 and figure 4. Cut-off size for each represented stage (i.e. left-end of coloured bars) are reported in the legend.

Table 1: geometric mean aerodynamic diameter (GMAD), relative mass concentration (RMC), and relative number of cases of mode presence (n.cases) for Aitken, condensation, droplet, coarse modes and very large particles. RMC evaluation was limited to the cases in which the mode was present.

	Aitken mode			Condensation mode			Droplet mode			Coarse mode			Very large particles		
	GMAD (μm)	RMC (%)	n. cases (%)	GMAD (μm)	RMC (%)	n. cases (%)	GMAD (μm)	RMC (%)	n. cases (%)	GMAD (μm)	RMC (%)	n. cases (%)	GMAD (μm)	RMC (%)	n. cases (%)
S				0.28	30%	86%	0.66	59%	100%	3.4	17%	71%			
Cl				0.36	18%	86%	0.72	29%	71%	4.4	61%	100%	16.1	10%	36%
K				0.26	31%	86%	0.58	46%	100%	3.7	25%	100%	15.7	9%	29%
Ca										3.9	79%	100%	15.7	11%	86%
Ti				0.22	5%	36%				3.5	71%	100%	15.1	13%	64%
Cr				0.31	17%	36%	0.67	38%	57%	2.9	64%	100%	4.7	29%	29%
Mn				0.30	13%	43%	0.72	42%	100%	3.2	50%	100%	15.7	10%	21%
Fe				0.42	6%	21%				3.2	74%	100%	16.6	7%	43%
Ni				0.28	21%	43%	0.48	45%	86%	3.0	50%	93%			
Cu				0.27	6%	71%				3.0	72%	100%	16.3	7%	21%
Zn				0.27	14%	79%	0.77	49%	93%	2.7	43%	100%	14.5	9%	14%
Levoglucosan	0.10	4%	100%	0.32	56%	100%	0.63	43%	78%	1.6	5%	78%	5.2	3%	78%
K^+	0.10	4%	44%	0.29	49%	89%	0.62	37%	89%	1.9	4%	22%	4.1	12%	89%
NO_3^-	0.11	2%	100%	0.31	28%	100%	0.71	61%	100%	2.4	6%	67%	4.0	10%	56%
$SO_4^=$	0.10	4%	100%	0.29	31%	100%	0.67	52%	100%	1.69	8%	56%	4.5	10%	100%
NH_4^+	0.10	2%	89%	0.31	35%	100%	0.70	62%	100%	3.5	2%	44%	8.2	1%	67%

730

732 *Table 2: geometric mean aerodynamic diameter (GMAD) and mode relative mass contribution (RMC) to each factor.*

Factor name		Aitken mode	Condensation submode	Droplet submode	Coarse mode	Very large particles
Wood Burning	GMAD (µm)	0.036	0.210	0.599		
	Relative contribution	4%	24%	72%		
Industry	GMAD (µm)	0.105	0.298		1.31	6.39
	Relative contribution	6%	58%		17%	19%
Resuspended Dust	GMAD (µm)		0.292	0.586	2.99	9.15
	Relative contribution		33%	23%	34%	10%
Regional	GMAD (µm)		0.203	0.695	2.81	
	Relative contribution		9%	81%	10%	
Construction works	GMAD (µm)	0.034	0.189	0.567	2.61	7.53
	Relative contribution	11%	14%	25%	12%	37%
Traffic 1	GMAD (µm)	0.118	0.344	0.98	2.97	9.30
	Relative contribution	5%	28%	33%	23%	12%
Traffic 2	GMAD (µm)	0.094	0.286	0.823	4.18	
	Relative contribution	7%	31%	38%	24%	

733

Histogram representation

a)

Micron inversion

b)

Modes retrieval

c)
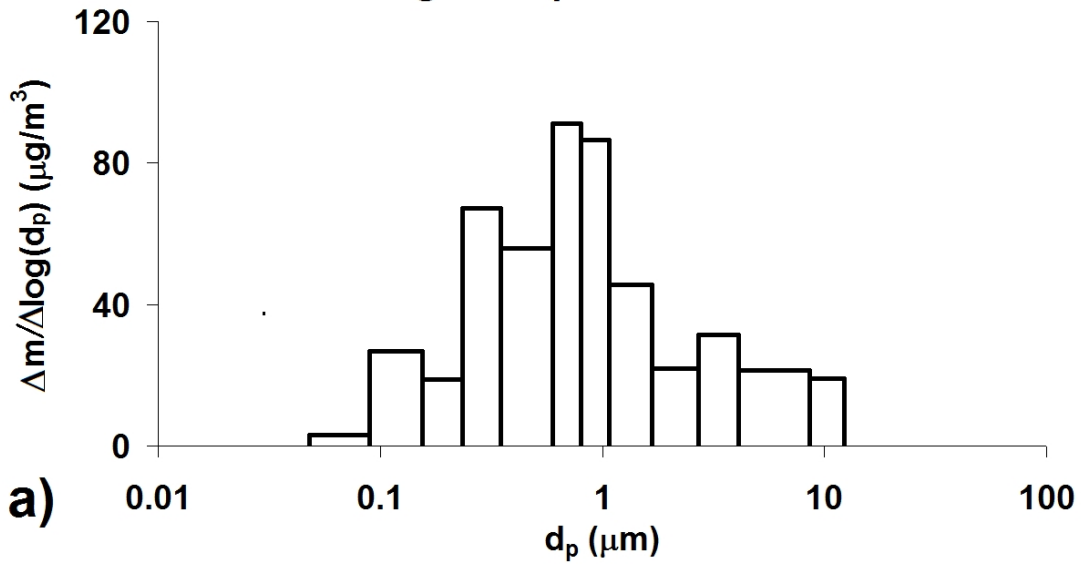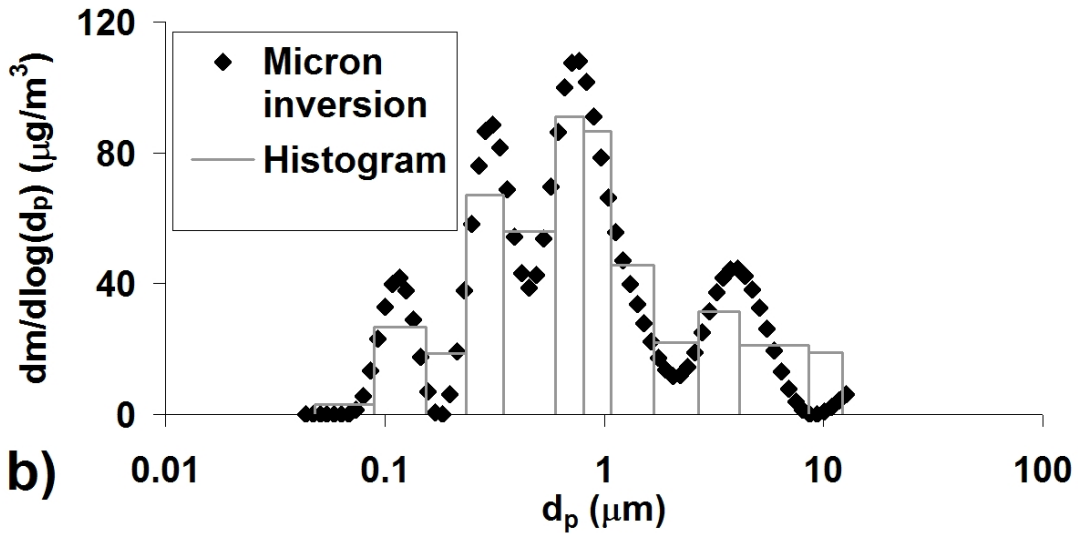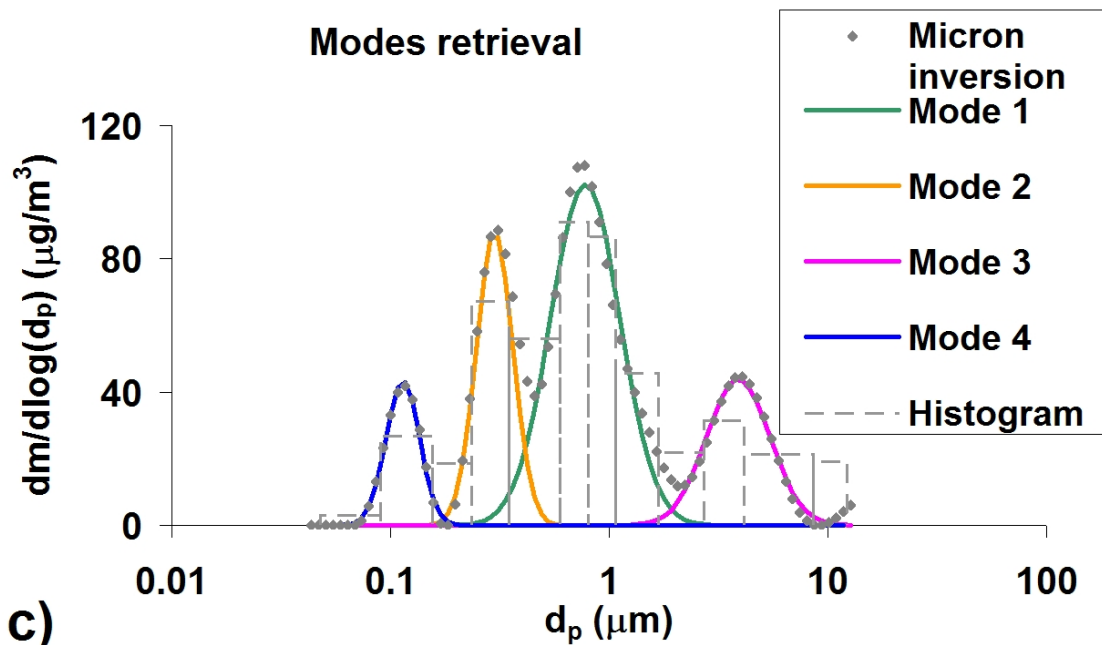
Average mass size distribution
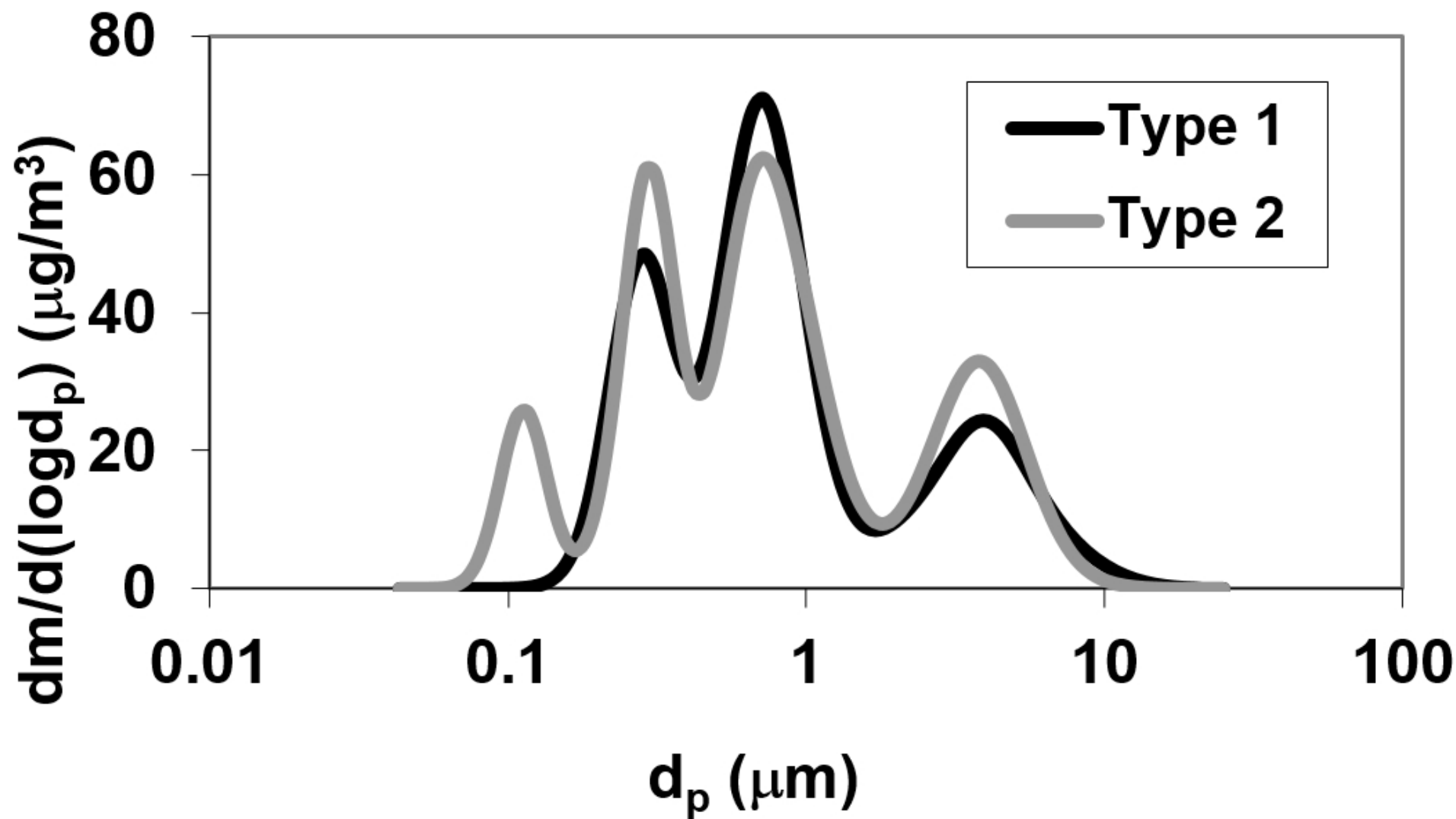
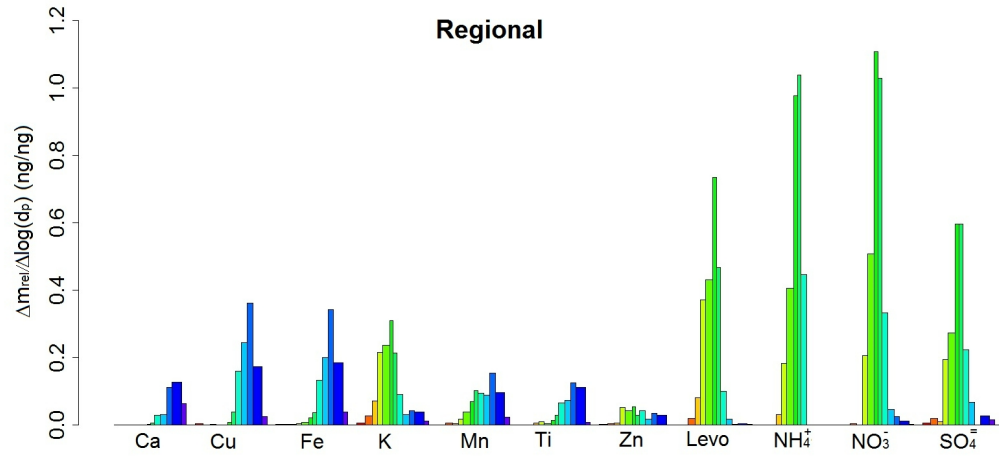# Secondary inorganic ions: average size distribution
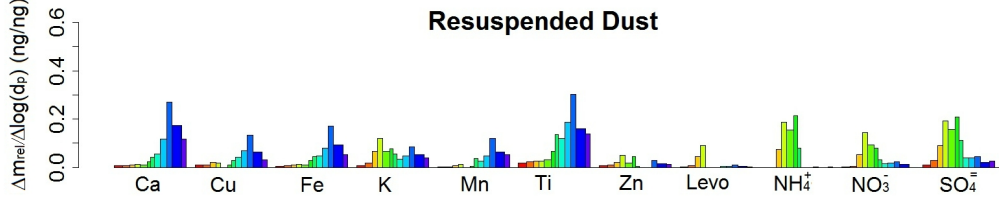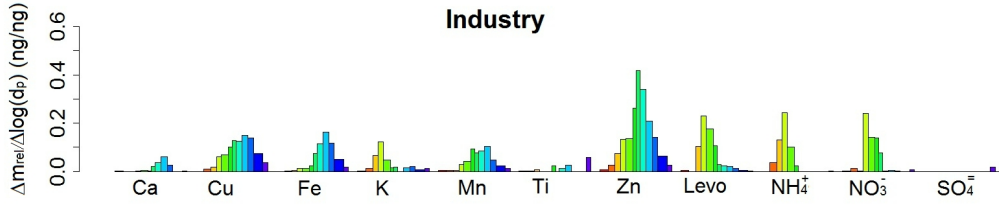

a)

Wood burning markers: average size distribution

b)

Traffic markers: average size distribution

c)

Wood Burning

Industry

Resuspended Dust

Regional

Construction Works

Traffic 1

Traffic 2

Wood Burning

Industry

Resuspended Dust

Regional

Construction works

Traffic 1

Traffic 2

Cut-off diameter (μm)

0.048	0.235	0.804	2.70
0.090	0.349	1.07	4.12
0.155	0.598	1.68	8.57

AITKEN MODE

- Resuspended dust, 0%
- Regional aerosol, 0%
- Wood Burning, 15%
- Traffic 1, 24%
- Traffic 2, 17%
- Construction works, 32%
- Industry, 12%

CONDENSATION MODE

- Regional aerosol, 12%
- Industry, 18%
- Construction works, 6%
- Resuspended dust, 18%
- Traffic 2, 13%
- Wood Burning, 12%
- Traffic 1, 21%

DROPLET MODE

- Wood Burning, 19%
- Traffic 1, 12%
- Traffic 2, 8%
- Construction works, 6%
- Resuspended dust, 6%
- Regional aerosol, 50%
- Industry, 0%

COARSE MODE AND VERY LARGE PARTICLES

- Industry, 11%
- Regional aerosol, 11%
- Resuspended dust, 22%
- Construction works, 22%
- Wood Burning, 0%
- Traffic 2, 9%
- Traffic 1, 25%

Cu

Mn

Zn

Cut-off diameter (μm)

■ 0.048	■ 0.235	■ 0.804	■ 2.70
■ 0.090	■ 0.349	■ 1.07	■ 4.12
■ 0.155	■ 0.598	■ 1.68	■ 8.57